

Coarse-to-Fine Monocular Re-Localization in OpenStreetMap via Semantic Alignment

Yuchen Zou, Xiao Hu*, Dexing Zhong, Yuqing Tang

Abstract—Monocular re-localization plays a crucial role in enabling intelligent agents to achieve human-like perception. However, traditional methods rely on dense maps, which face scalability limitations and privacy risks. OpenStreetMap (OSM), as a lightweight map that protects privacy, offers semantic and geometric information with global scalability. Nonetheless, there are still challenges in using OSM for localization: the inherent cross-modal discrepancies between natural images and OSM, as well as the high computational cost of global map-based localization. In this paper, we propose a hierarchical search framework with semantic alignment for localization in OSM. First, the semantic awareness capability of DINO-ViT is utilised to deconstruct visual elements to establish semantic relationships with OSM. Second, a coarse-to-fine search paradigm is designed to replace global dense matching, enabling efficient progressive refinement. Extensive experiments demonstrate that our method significantly improves both localization accuracy and speed. When trained on a single dataset, the 3° orientation recall of our method even outperforms the 5° recall of state-of-the-art methods.

I. INTRODUCTION

Empowering intelligence with human-like perception capability has been a central goal of intelligent systems [1]. As one of the core technologies, monocular visual relocation estimates the pose through a single image input. This enables it to show unique advantages in scenarios such as navigation [2], autonomous driving [3] and virtual reality [4]–[6]. Compared to LiDAR or multi-ocular stereo vision solutions, monocular systems offer lower hardware costs and greater deployment flexibility. Therefore, it is widely applicable in commercial processes.

Traditional monocular re-location methods usually rely on pre-constructed dense point cloud maps [7] or reference image databases [8], [9]. However, these methods face two main challenges: i) the cost of constructing and updating high-precision maps grows exponentially with scene size [10]; ii) there is a risk of privacy leakage from sensitive geographic information during acquisition [11]. OpenStreetMap (OSM)-based open source vector map offer a breakthrough solution to these challenges - OSM continuously updates landmark features such as road topology and building profile [12], providing rich semantic and structured prior knowledge for localization [13]. In addition, vector representations in OSM are lightweight and privacy-friendly.

However, achieving accurate monocular localization on OSM is far from straightforward. First, monocular images

Y. Zou and D. Zhong are with the School of Automation Science and Engineering, Xi'an Jiaotong University, Xi'an, Shaanxi 710049, China
X. Hu and Y. Tang are with the International Digital Economy Academy, Guangdong, Shenzhen 510085, China

* Corresponding author (e-mail: huxiao1@idea.edu.cn)

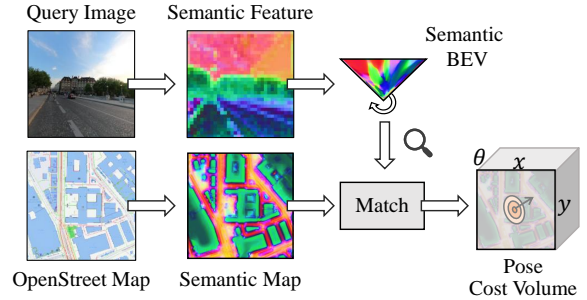


Fig. 1. Localization in the OSM-derived semantic map by transforming the query image into semantic features.

typically capture surface textures, lighting, and viewpoint variations from pedestrian view. In contrast, map data provides structured spatial information from a top-down view, such as road networks and building outlines. The modality gap makes direct matching between the image and the map extremely challenging. Moreover, in large-scale environments, performing fine-grained search across OSM is not only computationally expensive but also constrained by real-time performance requirements [14].

To address these challenges, we re-examine the OSM-based localization task. The core of task lies in aligning the visual information in monocular images with the semantic geometric elements in the OSM. Therefore, the key to improving localization performance is the effective decoupling of semantic information (such as buildings, roads, etc.) in the image.

Inspired by the powerful potential of DINO [15] in capturing high-level semantics, we leverage DINO-ViT to separate visual features for alignment with the semantic elements in OSM. As shown in Fig. 1, the query image is separated into visual features with different semantics by DINO. Then the OSM tile is converted into a semantic map with the same semantic dimensions to align the semantics. Furthermore, we depart from traditional fine-grained exhaustive search [14], [16], proposing a coarse-to-fine search strategy. This strategy gradually progressively refines the viewing direction and map position, significantly reducing computational complexity while ensuring high accuracy.

The main contributions are summarized as follows:

- By leveraging DINO-ViT's powerful semantic understanding capabilities, we efficiently align the complex features in monocular images with the geometric elements in OSM.
- A coarse-to-fine OSM-based localization framework is

designed. By progressively refining the inferred location in OSM, the framework improves both the speed and accuracy during localization.

- Extensive experiments were conducted on street view and autonomous driving datasets. Our method not only triples the localization speed, but also achieves a 3° orientation recall that outperforms the 5° recall of state-of-the-art methods.

II. RELATED WORK

A. Monocular Re-Localization

MRL utilizes low-cost monocular cameras to estimate the direction and location of an agent when revisiting previously mapped areas [17]. As a spatial model of an explored scene, the graph stores prior knowledge about the scene (e.g., appearance, geometry, topology, etc.). Among various approaches, ground image mapping remains the most commonly used solution. Place recognition via image retrieval allows for coarse localization based on a set of reference images [18]–[20]. To estimate precise pose, feature-matching algorithms typically require a 3D map [21]. However, 3D maps involve dense point clouds with high-dimensional visual descriptors, which demand substantial memory storage. Furthermore, there is a significant risk of personal data leakage within the map. In this context, OSM as an open-source vector map database, provides lightweight structural and semantic priors for visual localization. Compared to traditional maps, OSM vector representation significantly reduces memory usage and also mitigates potential data privacy risks [22]. Early studies assisted localization by matching road networks with information observed by the robot [23]–[25]. Some work also leveraged textual features from OSM for localization [26]. In the era of deep learning, OrienterNet [14] combines OSM’s structure and semantics into a semantic neural map and performs dense matching to estimate pose. However, due to perspectival and modality gaps, effectively aligning query images with map data remains extremely challenging. Additionally, performing dense matching across the entire OSM incurs significant computational costs.

B. Hierarchical Localization

In the field of visual localization, a widely used framework is Hierarchical Localization (HLoc), which follows a coarse-to-fine approach. This approach typically combines Visual Place Recognition (VPR) for reference image retrieval and coarse localization [27], followed by precise matching using visual landmarks. In HLoc [28], [29], the first stage performs global retrieval to generate location hypotheses, which are then refined through local feature matching to verify these candidate locations. Recently, coarse-to-fine localization methods based on neural maps have emerged to accelerate the registration process. In OSM, MapLocNet [30] employs a coarse-to-fine feature registration strategy to regress the location. However, MapLocNet is trained on a panoramic autonomous driving dataset. When applied to monocular street view images, directly regressing poses on a heterogeneous map like OSM becomes quite challenging. To alleviate this

modality gap, we employ a coarse-to-fine matching approach instead of directly regressing locations, while still enabling end-to-end training through pose supervision.

C. ViT Feature Representation

Vision Transformer (ViT) [31] has become a powerful and versatile visual representation model. Researchers have demonstrated that ViT trained in specific ways work well for numerous downstream tasks [32]–[34]. Among these, CLIP [33] uses natural semantics to describe visual content, which is frequently applied to text-driven semantic editing [35] and semantic segmentation [36]. Subsequently, DINO [15] as a self-supervised ViT model, has shown remarkable capabilities in capturing high-level semantic information [37]. Amir et al. [38] used the keys of DINO as features and applied them to challenging visual tasks in unconstrained environments. Numerous research has confirmed DINO’s robustness and generalization ability in complex scenes [20], [39], [40]. Given its success, we believe DINO can effectively decouple the semantics of complex street view images, enabling better alignment with the semantic information in OSM. In Section III, we will analyze DINO’s performance in street view feature extraction and compare it with classic feature extraction models.

III. DINO ON STREET VIEW

DINO is a ViT model trained through self-supervised learning with a unique dual-network architecture. In training process, the student network is optimized by minimizing the cross-entropy loss between the teacher network. The teacher network’s parameters are updated through an Exponential Moving Average (EMA) of the student’s parameters. This training mechanism allows DINO to exhibit excellent feature abstraction capabilities, especially in encoding high-level semantic information. Based on this characteristic, we expect DINO to extract semantic representations from street view images, facilitating reliable alignment with semantic maps like OSM.

To validate DINO’s capability in semantic representation of street view images, we conducted a visualization comparison of intermediate features from different models. As shown in Fig. 2, we input street view images into different architectures and visualized the feature maps or tokens using Principal Component Analysis (PCA). Each principal component corresponds to a specific color channel in the image. According to the PCA results, in simple scenes, both VGG [41], ResNet [42], and DINO [43] are able to effectively differentiate between the semantic information of buildings and roads. However, in more complex scenes (e.g., dense urban areas or textured road surfaces), VGG and ResNet primarily rely on local fine-grained features, which leads to confusion in the semantic information. In contrast, DINO is able to segment the street view image reasonably based on global semantics. It not only accurately distinguishes between buildings and roads but also effectively identifies fine-grained elements like street poles. Notably, buildings, roads, and street poles are represented as areas, lines, and

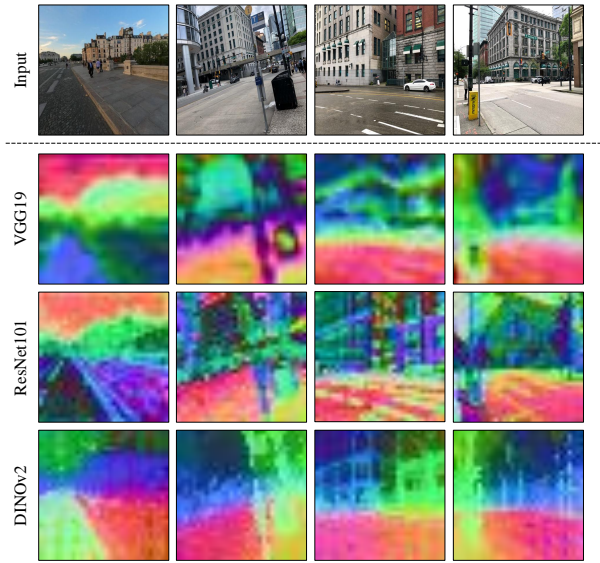


Fig. 2. Visualization of street view image features from VGG19, ResNet101, and DINOv2, where the same color represents the same semantics shared.

points in the OSM, respectively. Thus, the ability to precisely decouple these elements is crucial for achieving alignment with the OSM. Therefore, we chose to use DINO’s tokens as feature representations to build semantic links between cross-modal matching between vision and maps.

IV. METHOD

Given a single street view query image I and its coarse location, our goal is to estimate the position coordinates (x, y) and the heading angle θ to form a 3-DoF pose $\xi = (x, y, \theta)$. Such simplified pose representations are commonly used in practical localization, especially for outdoor ground scenes.

To perform queries in the OSM, we transform both the query image and the OSM tile into a unified semantic space. The overview of the proposed framework is illustrated in Fig. 3. First, we use DINO to extract the semantic features of the query image I and project them to the Bird’s-Eye View (BEV) space (Subsection A). Next, the OSM tile is rasterized according to different semantics to create a neural semantic map (Subsection B). Finally, the semantic BEVs are queried in the semantic map. To accelerate the matching process, we perform coarse pose sampling, and select the most probable pose for refinement (Subsection C).

A. Semantic BEV Projection

For the semantic transformation of query images, two core issues need to be addressed: i) decoupling different semantic information, and ii) transforming the pedestrian perspective image into a BEV perspective.

Since DINO demonstrates excellent performance in semantic differentiation of street view images, we adopt DINO to decouple different semantic elements (e.g., buildings, roads, etc.) in query image I . This provides a clearer semantic prior for subsequent map matching. In addition, the powerful cross-view capability of DINO enables to efficiently align

pedestrian viewpoint features with top-down map features. During the training process, we freeze the first 8 layers of the DINO encoder to maintain stable representations and reduce overfitting on the training dataset. The remaining 4 layers are fine-tuned to discard irrelevant semantic information (e.g., pedestrians, vehicles, etc.), further enhancing the model’s sensitivity to key elements in the scene (e.g., buildings and roads) to obtain the semantic feature $F_I \in \mathbb{R}^{U \times V \times N}$.

Next, the semantic feature is projected into the BEV space by relying on monocular reasoning, with reference to scale-distribution based BEV projection method [14]. Specifically, combining the camera’s intrinsic parameters, the semantic BEV representation is obtained in two steps: i) the semantic feature $F_I \in \mathbb{R}^{U \times V \times N}$ are converted into polar coordinates $F_{polar} \in \mathbb{R}^{U \times D \times N}$ by mapping image columns to radial rays. ii) the polar grid $F_{polar} \in \mathbb{R}^{U \times D \times N}$ is horizontally interpolated and resampled onto a Cartesian grid, mapping the feature to the BEV space $F_{bev} \in \mathbb{R}^{L \times D \times N}$. The projection process is represented as:

$$F_{polar}(u, d, n) = \sum_v \alpha_{(d,v)} \cdot F_I(u, v, n), \quad (1)$$

$$F_{bev}(l, d, n) = \sum_u \alpha_{(u,l)} \cdot F_{polar}(u, d, n), \quad (2)$$

where $\alpha_{(d,v)} \in [0, 1]$ is a depth-based probability distribution representing the interpolation weight between image column v and depth plane d , $\alpha_{(u,l)} \in [0, 1]$ is the horizontal interpolation ratio from the polar coordinate system to the Cartesian coordinate system, determined by the camera’s focal length and optical center.

B. Semantic Map Encoding

After obtaining the semantic projection F_{bev} of the street view image, it is necessary to convert the discrete OSM into a semantic neural map that can be matched. OSM provides multi-level vectorized annotations, including polygon elements representing building contours, polyline elements representing road topology, and point features representing Points of Interest (POI). These geometric elements not only provide direct geometric spatial constraints, but also assist in localization through their diverse semantic information. However, the original OSM data is in structured vector format, which has representational differences with raster-based deep learning frameworks. Therefore, it needs to be encoded into continuous neural map.

To address this, a local OSM tile with a $W \times H$ grid is first sliced based on the initial coarse position. Next, a semantic embedding matrix is built, mapping discrete categories to a continuous feature space through a learnable embedding layer. Finally, a neural semantic map $F_{map} \in \mathbb{R}^{W \times H \times N}$ is generated by the network, where each pixel represents the semantic information of the corresponding geographic region. The channel dimension N is aligned with the channel dimension of the F_{bev} . Following MapLocNet [30], we employ a U-Net architecture to efficiently utilize these features in the subsequent coarse-to-fine query process.

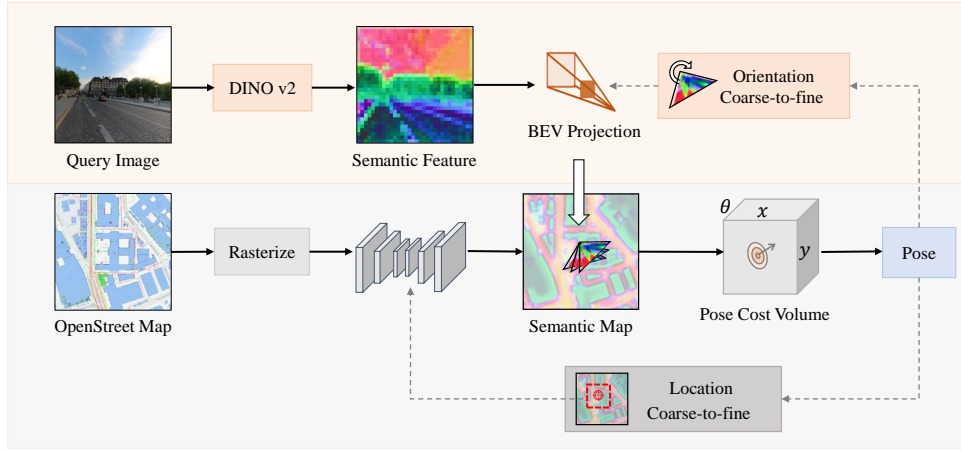


Fig. 3. Coarse-to-fine semantic localization framework for OSM localization. First, the query image is transformed into semantic features. Then, the sliced OSM tile is converted into a semantic map. A coarse pose is estimated through coarse semantic matching. Finally, based on the uncertainty of the coarse pose, a refined match is returned.

C. Coarse-to-Fine Pose Estimation

After obtaining the semantic BEV and semantic map, we estimate the discrete probability distribution of camera pose. According to the latest map-matching methods [14] [16], multiple directional hypotheses are typically constructed by rotating F_{bev} . Then, different locations in the map F_{map} are traversed for matching. By comparing the matching responses of each location, the hypothesis pose with the maximum response is selected as estimated camera pose.

However, performing dense global pose sampling leads to high computational costs, resulting in a trade-off between speed and accuracy. To address this, we employ a coarse-to-fine hierarchical matching strategy. Specifically, in the coarse matching phase, we first construct a coarse, discretized pose hypothesis space. For the coarse F_{bev}^c , rotational equivariant feature representations are generated using the orientation sampling matrix $R(\theta) \in SO(2)$:

$$F_{bev}^c(\theta) = R(\theta) \cdot F_{bev}^c, \quad \theta \in \{0, \Delta\theta^c, 2\Delta\theta^c, \dots, 2\pi\}, \quad (3)$$

where $\Delta\theta^c$ is the coarse sampling angular interval. Simultaneously, low-resolution map features $F_{map}^c \in \mathbb{R}^{H' \times W' \times N}$ are extracted from the intermediate layers of the decoding network. The coarse map F_{map}^c is used to construct the search space. A 3 Degrees-Of-Freedom (DOF) pose cost field is constructed via Fourier domain correlation operations:

$$M(p, \theta) = \sum_{(x,y) \in p} F^{-1} [F(F_{map}^c(p)) \odot F(F_{bev}^c(\theta))]_{(x,y)}, \quad (4)$$

where $F(\cdot)$ and $FFT^{-1}(\cdot)$ represent the Fourier transform and its inverse, respectively, and \odot is the element-wise conjugate multiplication operation. The coarse pose hypothesis is obtained via maximum likelihood estimation:

$$(p^c, \theta^c) = \arg \max_{(p \in P, \theta \in \Theta)} M(p, \theta). \quad (5)$$

After obtaining the optimal coarse estimates for position p^c and orientation hypothesis θ^c , pose fine-tuning is performed based on this prior information. Specifically, i) the direction estimate θ^c is used to construct a new rotational sampling window, adjusting the angular search range of F_{bev}^f ; ii) the position estimate p^c is used to establish spatial constraints, narrowing the sampling area on F_{map}^f . To achieve dynamic optimization of the sampling range, we introduce a pose uncertainty measure U , defined as:

$$U = \frac{1 - \exp(M(p^c, \theta^c))}{\sum_{(p, \theta) \in N(p^c, \theta^c)} \exp(M(p, \theta))}, \quad (6)$$

where $(p, \theta) \in N(p^c, \theta^c)$ represents the neighborhood pose hypotheses. Based on this measure, the search ranges for direction angle Θ^f and position P^f are dynamically adjusted:

$$\Theta^f = [\theta^* - k_\theta U \Delta\theta^f, \theta^* + k_\theta U \Delta\theta^f], \quad (7)$$

$$P^f = [p^* - k_p U, p^* + k_p U], \quad (8)$$

where k_θ and k_p control the extent of the range contraction for direction and position, and $\Delta\theta^f$ is the angular step size. In this way, the search range can be adaptively adjusted based on the uncertainty measure, improving the pose estimation accuracy. Fig. 4 visualizes the neural map and the matching process from coarse-to-fine.

V. EXPERIMENTS

A. Dataset

MGL Dataset: Mapillary platform provides a collection of images captured from various cameras and viewpoints. The dataset includes approximately 760,000 images from 12 cities across Europe and the United States, offering diverse viewpoints and different shooting environments. Each image is accompanied by rich metadata, including camera type and parameters, 6-DOF poses, shooting location coordinates, timestamp, and potentially noisy GPS coordinates. All imagery is available via the Mapillary API and is licensed under

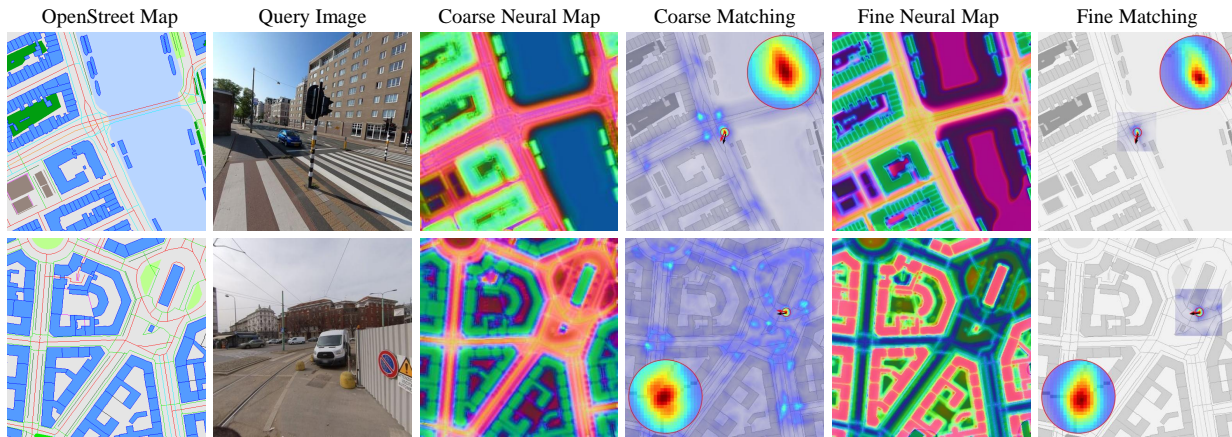


Fig. 4. Visualization of the coarse-to-fine localization process, including refinement of the neural map transformed from OSM, and refinement of the pose likelihood during matching. The red arrow represents the predicted pose, and the black arrow represents the ground truth pose.

a CC-BY-SA licence. To be fair, images are acquired at Mapillary using image IDs provided by [14]. OSM tiles are acquired from the noisy GPS position information attached to the MGL image.

KITTI Dataset: KITTI dataset [44] provides multi-modal sensor data from autonomous vehicles. Each frame is accompanied by detailed metadata, including camera parameters, 6-DOF poses, GPS coordinates, IMU measurements, and LiDAR point clouds. Following in [14], [45], the Test2 Split is used, ensuring no overlap between KITTI and MGL training sets. OSM tiles are acquired by sampling 20m centred around the GPS position information attached to the KITTI image.

B. Implementation Details

We use the DINOv2 with register [43] for semantic extraction. For OSM, we divide the region of into 7 categories for areas, 10 categories for roads, and 33 categories for points. We employ VGG16 to convert the rasterized map into a neural semantic map and add a decoder head. For the coarse matching phase, the map resolution is set to 1 meter, with an angular interval of 6° . In the fine matching phase, the resolution is increased to 0.5 meters, and the angular interval is reduced to 2° . During training, sample points are randomly selected within a 32-meter radius centered around the ground truth pose, without applying any pose constraints. In the testing phase, for MGL dataset, we do not use pose prior and directly query poses on the 128×128 meter OSM tile. For KITTI dataset, we incorporate prior pose during testing, with sample points selected within a $\pm 10^\circ$ range of initial pose. All experiments are performed using three NVIDIA RTX 4090 GPUs.

VI. COMPARISON METHODS

We compare the proposed method with previously published monocular localization methods, specifically including: i) Retrieval Methods [46], [27]: utilize high-density map patch retrieval through neural map correlation and global image embedding for BEV reasoning and matching. ii)

TABLE I
PERFORMANCE OF MGL DATASET FOR LOCALIZATION IN STREET SCENE. 'C' DENOTES COARSE LOCALIZATION AND 'F' DENOTES FINE LOCALIZATION.

Method	Position R@Xm			Orientation R@X $^\circ$			FPS
	1m	3m	5m	1 $^\circ$	3 $^\circ$	5 $^\circ$	
Retrieval	2.02	15.21	24.21	4.50	18.61	32.48	-
Refinement	8.09	26.02	35.31	14.92	36.87	45.19	-
OrienterNet	15.78	47.75	58.98	22.14	52.56	66.32	7.51
Ours-C	14.70	49.58	64.43	23.26	59.75	78.99	29.54
Ours-F	17.36	53.67	65.81	30.66	68.71	80.53	25.80

Refinement Methods [45], [47]: update the initial pose by distorting satellite views to match the image. iii) OrienterNet [14]: performs BEV transformation on images for intensive matching with OSM data. To the best of our knowledge, although there have been updated methods based on OSM localization [30], these are trained on surround-view autonomous driving datasets. Our attempt to use single-view training did not yield satisfactory results. Among existing methods, OrienterNet is the state-of-the-art monocular localization method based on OSM, with the code publicly available.

A. MGL Result

Through quantitative evaluation of the performance of different methods, we provide a comprehensive comparison in terms of position recall rate, orientation recall rate, and Frames Per Second (FPS). As shown in Table I, our method demonstrates significant improvements in both accuracy and speed. Specifically, coarse localization significantly enhances localization efficiency, while fine localization effectively improves pose estimation accuracy. In terms of efficiency, we improve the speed of localization by more than a three-fold. In terms of accuracy, this strategy is particularly effective in terms of orientation recall. Compared to the advanced OrienterNet method, which was trained with an orientation resolution of 5.625° , our method achieves a finer orientation

TABLE II

PERFORMANCE OF KITTI DATASET FOR LOCALIZATION IN DRIVING SCENARIOS. THE USED MAPS ARE FROM SATELLITE AND OSM. THE USED TRAINING DATASETS CONSIST OF KITTI DATASET AND MGL WITH KITTI MIXED DATASET.

Map	Method	Train dataset	Lateral R@Xm			Longitudinal R@Xm			Orientation R@X°		
			1m	3m	5m	1m	3m	5m	1°	3°	5°
Satellite	DSM [48]	KITTI	10.77	31.37	48.24	3.87	11.73	19.50	3.53	14.09	23.95
	VIGOR [49]	KITTI	17.38	48.20	70.79	4.07	12.52	20.14	5.46	15.79	27.15
	Refinement [45]	KITTI	27.82	59.79	72.89	5.75	16.32	26.48	18.42	49.72	71.00
OSM	OrienterNet [14]	KITTI	51.26	84.77	91.81	22.39	46.79	57.81	20.41	52.24	73.53
	Ours	KITTI	68.05	92.84	95.81	27.45	57.89	68.34	37.28	80.16	92.12
	OrienterNet [14]	MGL+KITTI	65.91	92.76	96.54	33.07	65.18	75.15	35.72	77.49	91.51
	Ours	MGL+KITTI	72.28	94.42	97.49	37.87	71.40	79.61	42.83	87.26	96.37

TABLE III

IMPACT OF DINO COMPONENT AND COARSE-TO-FINE (C2F) MATCHING STRATEGY ON LOCALIZATION PERFORMANCE.

Method	Position R@Xm			Orientation R@X°			FPS
	1m	3m	5m	1°	3°	5°	
Baseline	14.37	48.69	61.7	20.95	54.96	70.17	7.34
+ DINO	17.06	53.17	65.31	24.54	61.28	76.35	6.81
+ C2F	17.36	53.67	65.81	30.66	68.71	80.53	25.80

resolution of 2°. This results in a significant improvement in orientation accuracy. With this finer search strategy, our method outperforms the state-of-the-art method by 38.48% in terms of 1° recall.

B. KITTI Result

On KITTI dataset, we followed the method from [14] and employed two training strategies: i) training the model from scratch using KITTI dataset, and ii) fine-tuning the model pre-trained on MGL dataset. We compared our method with the satellite-based and OSM-based localization approaches. Benefiting from the powerful zero-shot semantic perception of the DINO model, our method performs particularly well on KITTI dataset, which has a smaller training set. As shown in Table II, our method significantly outperforms others in both lateral/longitudinal position recall and orientation recall. Notably, when training on KITTI dataset, the recall rate at 3m/3° even outperforms that of state-of-the-art method at 5m/5°.

VII. ABLATION STUDIES

In order to evaluate the contribution of each component, we conducted ablation experiments, including the role of adding DINO and coarse-to-fine matching strategy. The baseline is the feature extraction model of ResNet101 using global fine matching strategy. The ablation results are shown in Table III. After incorporating DINO, the model demonstrated significant improvements in localization accuracy. This result indicates that DINO’s advantages in semantic awareness effectively enhanced the semantic consistency between images and OSM. However, there was a slight decrease in computational efficiency. When the coarse-to-fine strategy was further introduced, both positioning accu-

racy and efficiency improved significantly. Notably, in the high-precision orientation estimation task, the recall rate of orientation is greatly improved. Moreover, FPS increased by more than threefold, demonstrating the significant advantage of the coarse-to-fine strategy in optimizing computational efficiency.

VIII. CONCLUSION

In this paper, we proposed a hierarchical localization method with semantic alignment, capable of efficiently querying the 3-DOF pose of a single image from OSM. By leveraging the powerful semantic understanding capabilities of DINO-ViT model, we facilitated the semantic alignment between street view image and OSM data. Additionally, a coarse-to-fine matching strategy is designed to balance the localization accuracy and query efficiency. Through extensive experiments on MGL and KITTI datasets, our method significantly outperformed existing approaches in re-localization performance. Notably, the 3° orientation recall of our method even outperforms the 5° recall of state-of-the-art methods. The proposed method combines semantic geometric reasoning with resource-efficient search, offering a solution for privacy-sensitive urban localization.

REFERENCES

- [1] L. Liang, G. Bian, H. Zhao, Y. Dong, and H. Liu, “Extracting dynamic navigation goal from natural language dialogue,” in *IROS*, 2023, pp. 3539–3545.
- [2] D. Maggio, M. Abate, J. Shi, C. Mario, and L. Carlone, “Loc-nerf: Monte carlo localization using neural radiance fields,” in *ICRA*. IEEE, 2023, pp. 4018–4025.
- [3] T. Wen, K. Jiang, B. Wijaya, H. Li, M. Yang, and D. Yang, “Tm³loc: Tightly-coupled monocular map matching for high precision vehicle localization,” *IEEE Trans. Intell. Transp. Syst.*, vol. 23, no. 11, pp. 20268–20281, 2022.
- [4] M. Smith, J. L. Gabbard, G. Burnett, C. Hare, H. Singh, and L. Skrypchuk, “Determining the impact of augmented reality graphic spatial location and motion on driver behaviors,” *Applied ergonomics*, vol. 96, p. 103510, 2021.
- [5] Y. S. W. W. Arachchige, H. K. Lukosch, J. Everett, and S. Lukosch, “Representing remote locations with location-based augmented reality game design,” *Entertainment Computing*, p. 100932, 2025.
- [6] J. Miao, K. Jiang, T. Wen, Y. Wang, P. Jia, B. Wijaya, X. Zhao, Q. Cheng, Z. Xiao, J. Huang, *et al.*, “A survey on monocular re-localization: From the perspective of scene map representation,” *IEEE Transactions on Intelligent Vehicles*, 2024.
- [7] Y. Xia, L. Shi, Z. Ding, J. F. Henriques, and D. Cremers, “Text2loc: 3d point cloud localization from natural language,” in *CVPR*. IEEE, 2024, pp. 14958–14967.

- [8] S. Garg, T. Fischer, and M. Milford, "Where is your place, visual place recognition?" in *IJCAI*, 2021, pp. 4416–4425.
- [9] K. A. Tsintotas, L. Bampis, and A. Gasteratos, "The revisiting problem in simultaneous localization and mapping: A survey on visual loop closure detection," *IEEE Trans. Intell. Transp. Syst.*, vol. 23, no. 11, pp. 19 929–19 953, 2022.
- [10] G. Elghazaly, R. Frank, S. Harvey, and S. Safko, "High-definition maps: Comprehensive survey, challenges, and future perspectives," *IEEE Open Journal of Intelligent Transportation Systems*, vol. 4, pp. 527–550, 2023.
- [11] J. Zhu, S. Yan, L. Wang, S. Zhang, Y. Liu, and M. Zhang, "Lod-loc: Aerial visual localization using lod 3d map with neural wireframe alignment," in *NeurIPS*, 2024.
- [12] OSMstats, "Osmstats - statistics of the free wiki world map." [Online]. Available: <https://osmstats.neis-one.org/>
- [13] C. Ho, J. Zou, O. Alama, S. M. J. Kumar, B. Chiang, T. Gupta, C. Wang, N. Keetha, K. Sycara, and S. Scherer, "Map it anywhere (mia): Empowering bird's eye view mapping using large-scale public data," in *Advances in Neural Information Processing Systems*, 2024.
- [14] P. Sarlin, D. DeTone, T. Yang, A. Avetisyan, J. Straub, T. Malisiewicz, S. R. Bulò, R. A. Newcombe, P. Kotschieder, and V. Balntas, "Orienternet: Visual localization in 2d public maps with neural matching," in *CVPR*, 2023, pp. 21 632–21 642.
- [15] M. Oquab, T. Darcet, T. Moutakanni, H. V. Vo, M. Szafraniec, V. Khalidov, P. Fernandez, D. Haziza, F. Massa, A. El-Nouby, M. Assran, N. Ballas, W. Galuba, R. Howes, P. Huang, S. Li, I. Misra, M. Rabbat, V. Sharma, G. Synnaeve, H. Xu, H. Jégou, J. Mairal, P. Labatut, A. Joulin, and P. Bojanowski, "Dinov2: Learning robust visual features without supervision," *Trans. Mach. Learn. Res.*, vol. 2024, 2024.
- [16] A. B. Camilletto, A. Bochicchio, A. Liniger, D. Dai, and A. Gawel, "U-BEV: height-aware bird's-eye-view segmentation and neural map-based relocalization," in *IROS*. IEEE, 2024, pp. 5597–5604.
- [17] N. Piasco, D. Sidibé, C. Demonceaux, and V. Gouet-Brunet, "A survey on visual-based localization: On the benefit of heterogeneous data," *Pattern Recognit.*, vol. 74, pp. 90–109, 2018.
- [18] R. Arandjelovic, P. Gronát, A. Torii, T. Pajdla, and J. Sivic, "Netvlad: CNN architecture for weakly supervised place recognition," *IEEE Trans. Pattern Anal. Mach. Intell.*, vol. 40, no. 6, pp. 1437–1451, 2018.
- [19] K. Garg, S. S. Puligilla, S. Kolathaya, K. M. Krishna, and S. Garg, "Revisit anything: Visual place recognition via image segment retrieval," in *ECCV (68)*, ser. Lecture Notes in Computer Science, vol. 15126, 2024, pp. 326–343.
- [20] N. V. Keetha, A. Mishra, J. Karhade, K. M. Jatavallabhula, S. A. Scherer, K. M. Krishna, and S. Garg, "Anyloc: Towards universal visual place recognition," *IEEE Robotics Autom. Lett.*, vol. 9, no. 2, pp. 1286–1293, 2024.
- [21] T. Sattler, B. Leibe, and L. Kobbelt, "Improving image-based localization by active correspondence search," in *ECCV (1)*, vol. 7572, 2012, pp. 752–765.
- [22] J. E. Vargas-Munoz, S. Srivastava, D. Tuia, and A. X. Falcao, "Openstreetmap: Challenges and opportunities in machine learning and remote sensing," *IEEE Geoscience and Remote Sensing Magazine*, vol. 9, no. 1, pp. 184–199, 2020.
- [23] G. Floros, B. van der Zander, and B. Leibe, "Openstreetslam: Global vehicle localization using openstreetmaps," in *ICRA*, 2013, pp. 1054–1059.
- [24] C. Mandel and O. Birbach, "Localization in urban environments by matching sensor data to map information," in *European Conference on Mobile Robots*, 2013, pp. 50–55.
- [25] B. Suger and W. Burgard, "Global outer-urban navigation with openstreetmap," in *ICRA*, 2017, pp. 1417–1422.
- [26] N. Radwan, G. D. Tipaldi, L. Spinello, and W. Burgard, "Do you see the bakery? leveraging geo-referenced texts for global localization in public maps," in *ICRA*, 2016, pp. 4837–4842.
- [27] Z. Xia, O. Booij, M. Manfredi, and J. F. Kooij, "Visual cross-view metric localization with dense uncertainty estimates," in *ECCV*, 2022, pp. 90–106.
- [28] P. Sarlin, F. Debraine, M. Dymczyk, and R. Siegwart, "Leveraging deep visual descriptors for hierarchical efficient localization," in *CoRL*, vol. 87, 2018, pp. 456–465.
- [29] P. Sarlin, C. Cadena, R. Siegwart, and M. Dymczyk, "From coarse to fine: Robust hierarchical localization at large scale," in *CVPR*, 2019, pp. 12 716–12 725.
- [30] H. Wu, Z. Zhang, S. Lin, X. Mu, Q. Zhao, M. Yang, and T. Qin, "Maplocnet: Coarse-to-fine feature registration for visual relocalization in navigation maps," in *IROS*, 2024, pp. 13 198–13 205.
- [31] A. Dosovitskiy, L. Beyer, A. Kolesnikov, D. Weissenborn, X. Zhai, T. Unterthiner, M. Dehghani, M. Minderer, G. Heigold, S. Gelly, *et al.*, "An image is worth 16x16 words: Transformers for image recognition at scale," in *ICLR*, 2021.
- [32] M. Caron, H. Touvron, I. Misra, H. Jégou, J. Mairal, P. Bojanowski, and A. Joulin, "Emerging properties in self-supervised vision transformers," in *ICCV*, 2021, pp. 9630–9640.
- [33] A. Radford, J. W. Kim, C. Hallacy, A. Ramesh, G. Goh, S. Agarwal, G. Sastry, A. Askell, P. Mishkin, J. Clark, G. Krueger, and I. Sutskever, "Learning transferable visual models from natural language supervision," in *ICML*, vol. 139, 2021, pp. 8748–8763.
- [34] N. Tumanyan, O. Bar-Tal, S. Bagon, and T. Dekel, "Splicing vit features for semantic appearance transfer," in *CVPR*, 2022, pp. 10 738–10 747.
- [35] O. Patashnik, Z. Wu, E. Shechtman, D. Cohen-Or, and D. Lischinski, "Styleclip: Text-driven manipulation of stylegan imagery," in *ICCV*, 2021, pp. 2065–2074.
- [36] C. Zhou, C. C. Loy, and B. Dai, "Extract free dense labels from CLIP," in *ECCV*, vol. 13688, 2022, pp. 696–712.
- [37] M. Wysoczanska, O. Siméoni, M. Ramamonjisoa, A. Bursuc, T. Trzcinski, and P. Pérez, "Clip-dinoiser: Teaching CLIP a few DINO tricks for open-vocabulary semantic segmentation," in *ECCV*, vol. 15119, 2024, pp. 320–337.
- [38] S. Amir, Y. Gandelsman, S. Bagon, and T. Dekel, "Deep vit features as dense visual descriptors," *arXiv preprint arXiv:2112.05814*, 2021.
- [39] J. Edstedt, Q. Sun, G. Bökman, M. Wadenbäck, and M. Felsberg, "Roma: Robust dense feature matching," in *CVPR*, 2024, pp. 19 790–19 800.
- [40] H. Jiang, A. Karpur, B. Cao, Q. Huang, and A. Araújo, "Omniglu: Generalizable feature matching with foundation model guidance," in *CVPR*, 2024, pp. 19 865–19 875.
- [41] K. Simonyan and A. Zisserman, "Very deep convolutional networks for large-scale image recognition," in *ICLR*, 2015.
- [42] K. He, X. Zhang, S. Ren, and J. Sun, "Deep residual learning for image recognition," in *CVPR*, 2016, pp. 770–778.
- [43] T. Darcet, M. Oquab, J. Mairal, and P. Bojanowski, "Vision transformers need registers," in *ICLR*, 2024.
- [44] A. Geiger, P. Lenz, C. Stiller, and R. Urtasun, "Vision meets robotics: The KITTI dataset," *Int. J. Robotics Res.*, vol. 32, no. 11, pp. 1231–1237, 2013.
- [45] Y. Shi and H. Li, "Beyond cross-view image retrieval: Highly accurate vehicle localization using satellite image," in *CVPR*, 2022, pp. 16 989–16 999.
- [46] N. Samano, M. Zhou, and A. Calway, "You are here: Geolocation by embedding maps and images," in *ECCV*, vol. 12368, 2020, pp. 502–518.
- [47] P. Sarlin, A. Unagar, M. Larsson, H. Germain, C. Toft, V. Larsson, M. Pollefeys, V. Lepetit, L. Hammarstrand, F. Kahl, and T. Sattler, "Back to the feature: Learning robust camera localization from pixels to pose," in *CVPR*, 2021, pp. 3247–3257.
- [48] Y. Shi, X. Yu, D. Campbell, and H. Li, "Where am I looking at? joint location and orientation estimation by cross-view matching," in *CVPR*, 2020, pp. 4063–4071.
- [49] S. Zhu, T. Yang, and C. Chen, "Vigor: Cross-view image geolocalization beyond one-to-one retrieval," in *CVPR*, 2021, pp. 3640–3649.